Journal of Microscopy, Vol. 227, Pt 1 2007, pp. 15–23
Received 6 July 2006; accepted 31 January 2007

Dynamic evaluation of autofocusing for automated microscopic analysis of blood smear and pap smear

X. Y. LIU, W. H. WANG & Y. SUN
Advanced Micro and Nanosystems Laboratory, University of Toronto, 5 King's College Road, Toronto M5S 3G8, Canada

Key words. Autofocusing, automated microscopic diagnosis, blood smear, dynamic evaluation, Fibonacci search, microscopy, pap smear.

Summary

Autofocusing is a fundamental procedure towards automated microscopic evaluation of blood smear and pap smear samples for clinical diagnosis. This paper presents comparison results of 16 selected focus algorithms based on 8000 static bright-field images and 1600 dynamic autofocusing trials using 10 blood smear and pap smear samples. Besides static behaviour, dynamic autofocusing performance is introduced for ranking the 16 focus algorithms. The Fibonacci search algorithm is employed for controlling the *z*-motor of the microscope to reach the focus position that is determined by focus objective functions. Experimental results demonstrate that the variance algorithm provides the best overall performance. Together with our previously reported findings, it is demonstrated that the variance algorithm or the normalized variance algorithm is the optimal focus algorithm for non-fluorescence microscopy applications including pap smear and blood smear imaging.

Introduction

Manual microscopic examination of hundreds or thousands of blood smear and pap smear samples is routinely performed by cytotechnologists and pathologists in clinical and hospital laboratory environments. Pap smear, which is a sample with cervical cells on a glass slide, is the most important diagnostic technique for detecting pre-invasive cervical cancer. Peripheral blood smear provides information on the number and shape of blood cells for detecting blood-related diseases, such as anaemia and leukaemia.

Advances have been made to make smear interpretation more descriptive, paving the foundation to the realization of automated computer-assisted microscopic diagnosis (Simon *et al.*, 1986; Angulo & Flandrin, 2003). Fully automated microscopic diagnosis is advantageous in that it will not only alleviate the tremendous workload from medical professionals (e.g. each pap smear contains roughly 50,000 to 300,000 cells) and result in greater efficiency; but more importantly, an automated microscopic diagnostic system will be capable of encompassing expert knowledge from diverse specialties within pathology to detect a multitude of diseases or a comprehensive disease pattern. Towards the realization of fully automated microscopic diagnosis of blood and pap smear, bringing a sample into focus or autofocusing is a fundamental procedure to perform.

Although autofocusing is a long-standing research topic and many focus algorithms have been proposed, the selection of the optimal algorithm for specific experimental microscopy applications remains *ad hoc*. The autocorrelation algorithm (Vollath, 1987, 1988) was found to be the optimal focus algorithm for fluorescence microscopy applications (Santos *et al.*, 1997). We previously demonstrated that the normalized variance algorithm provided the best performance for several types of non-fluorescence samples under bright field, phase contrast, and differential interference contrast (Sun *et al.*, 2004).

This paper focuses on the determination of the optimal focus algorithm for pap smear and blood smear bright-field imaging through a systematic evaluation of 16 commonly used focus algorithms that were applied to 10 blood smear and pap smear samples. Based on an evaluation methodology that examines the static performance of focus algorithms, we have recently demonstrated that the variance algorithm provides the best overall static performance for pap and blood smear (Liu *et al.*, 2006). In order to evaluate the dynamic focusing performance of each algorithm, which is directly relevant to the implementation of automated microscopic diagnosis of blood and pap smear, the Fibonacci search algorithm was selected for controlling the *z*-directional motor (i.e. objective position) to reach the focus position that corresponds to the maximum value of the focus objective function. Besides the

Correspondence to: Yu Sun. Tel: +1 416 946 0549; Fax: +1 416 978 7753; e-mail: sun@mie.utoronto.ca

five ranking criteria for static evaluation (Sun *et al.*, 2004; Liu *et al.*, 2006), two new criteria (dynamic accuracy and dynamic repeatability) are introduced for dynamically evaluating the selected focus algorithms.

Materials and method

As shown in Fig. 1, 10 samples (five blood smears and five pap smears) were experimentally tested in this study. These representative samples were selected as they include a variety of information. The five blood smear samples were prepared in the Princess Margaret Hospital (Toronto, Canada), and the five pap smear samples were prepared in the Sunnybrook Health Sciences Centre and Women's College Hospital (Toronto, Canada). The thickness is 15–20 μm for the blood smear samples and 10–15 μm for the pap smear samples.

Figure 2 shows the experimental setup that consists of a motorized inverted microscope (Olympus IX81), a CMOS digital camera (Basler A601f) and a host computer (3.2 GHz CPU with 1.0 GB RAM) for image processing and motion control. The minimum vertical motion step of the microscope is 0.01 μm. The camera has a pixel size of 9.9 × 9.9 μm. An objective (Olympus LUCPlanFLN, 1.9 μm depth of field, NA 0.6 and 0.5 μm resolution) and the bright-field observation method were used. The total magnification of the observation system (objective, coupler and camera) is 40×. Multiplying this 40× magnification with the resolution of the objective (0.5 μm), one can confirm that the pixel size of the camera (9.9 μm) satisfies the Nyquist theorem. Thus, no frequency aliasing in image acquisition occurred.

For static evaluation, 10 image sets corresponding to the 10 samples were collected with a step of 0.25 μm. Each set contains 800 images (640 × 480), amounting to a total of 8000 still images that were processed using the 16 focus algorithms presented in the Focus Algorithms section. Besides static evaluation, the *z*-motor of the microscope was controlled in real time for studying the dynamic behaviour of the 16 algorithms. For each sample, 10 dynamic autofocusing trials were conducted for each focus algorithm, amounting to 1600 dynamic autofocusing trials.

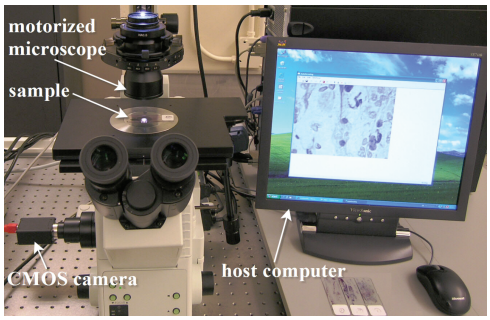

Fig. 2. System setup for investigating autofocusing of blood smear and pap smear samples.

Focus algorithms

A common rationale of focus algorithms is that focused images contain more information and details (e.g. edges) than unfocused images, based on which an objective function indicating the sharpness of images is used to evaluate the degree of focusing. The focus position is obtained when the objective function reaches its extremum. In this study, 16 focus algorithms that are most commonly used in the literature were compared to determine the optimal focus algorithm for pap smear and blood smear bright-field imaging. These algorithms are classified into four groups (Sun *et al.*, 2004). In order to make the paper self-contained and facilitate the discussion of results presented in the Experimental Results and Discussion section, the focus algorithms are briefly summarized as follows.

Derivative-based algorithms

Thresholded absolute gradient (Santos et al., 1997). The absolute value of first derivative is accumulated when it is larger than a

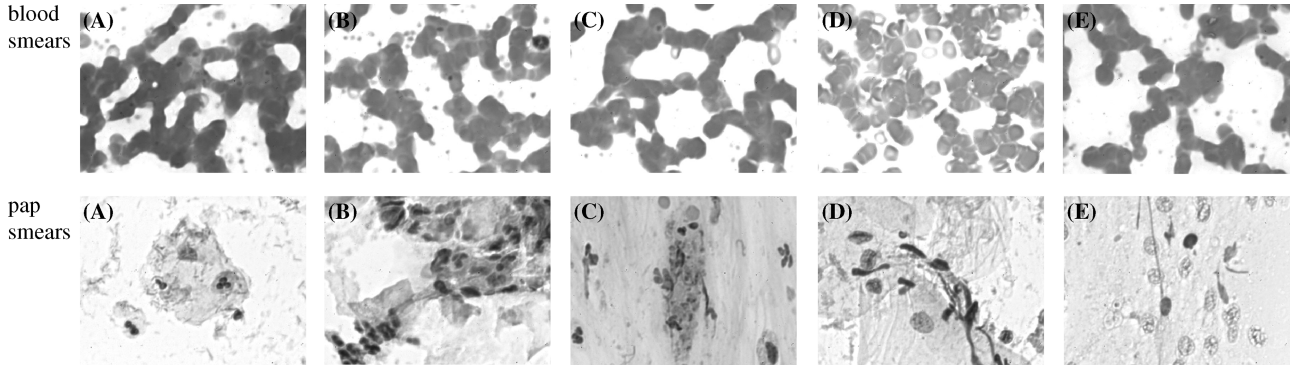

Fig. 1. Bright-field images of five blood smear samples (top) and five pap smear samples (bottom).

pre-defined threshold v:

$$f_{\text{thre\_grad}} = \sum_{\text{height}} \sum_{\text{width}} |i(x+1, y) - i(x, y)|, \quad (1)$$

where $i(x, y)$ is the grey level intensity of pixel (x, y), and $|i(x+1, y) - i(x, y)| \geq v$.

Squared gradient (Santos et al., 1997).

$$f_{\text{squa\_grad}} = \sum_{\text{height}} \sum_{\text{width}} (i(x+1, y) - i(x, y))^2, \quad (2)$$

where $(i(x+1, y) - i(x, y))^2 \geq v$.

Brenner gradient (Brenner et al., 1971).

$$f_{\text{Brenner}} = \sum_{\text{height}} \sum_{\text{width}} (i(x+2, y) - i(x, y))^2, \quad (3)$$

where $(i(x+2, y) - i(x, y))^2 \geq v$.

Tenenbaum gradient (Krotkov, 1987; Yeo et al., 1993).

$$f_{\text{Tenengrad}} = \sum_{\text{height}} \sum_{\text{width}} \left(S_x(x, y)^2 + S_y(x, y)^2\right), \quad (4)$$

where $S_x(x, y)$ and $S_y(x, y)$ are the convoluted images with Sobel operators.

Energy Laplace (Subbarao et al., 1993). The second derivative $C(x, y)$ is computed by convolving an image with the convolution mask:

$$L = \begin{bmatrix} -1 & -4 & -1 \\ -4 & 20 & -4 \\ -1 & -4 & -1 \end{bmatrix}$$

and the objective function is

$$f_{\text{energy\_Laplace}} = \sum_{\text{height}} \sum_{\text{width}} C(x, y)^2. \quad (5)$$

Sum of modified Laplace (Nayar & Nakagawa, 1994).

$$f_{\text{SML}} = \sum_{\text{height}} \sum_{\text{width}} \left(|L_x(x, y)| + |L_y(x, y)|\right), \quad (6)$$

where $L(x, y)$ are convoluted images with Laplacian operators.

Sum of squared Gaussian derivatives (Geusebroek et al., 2000).

$$f_{\text{sum\_Gaus\_deri}} = \frac{1}{MN} \sum_{\text{height}} \sum_{\text{width}} \left(G_x(\sigma)^2 + G_y(\sigma)^2\right), \quad (7)$$

where $G_x(\sigma)$ and $G_y(\sigma)$ are first-order Gaussian derivatives in horizontal/vertical directions. The scale can be determined by $\sigma = d/2\sqrt{3}$, where d is dimension of the smallest feature.

Statistical algorithms

Variance (Groen et al., 1985; Yeo et al., 1993).

$$f_{\text{variance}} = \frac{1}{H \cdot W} \sum_{\text{height}} \sum_{\text{width}} \left(i(x, y) - \bar{i}\right)^2, \quad (8)$$

where $\bar{i}$ is the mean intensity of the image, and H and W are image height and width.

Normalized variance (Groen et al., 1985; Yeo et al., 1993).

$$f_{\text{norm\_vari}} = \frac{1}{H \cdot W \cdot \bar{i}} \sum_{\text{height}} \sum_{\text{width}} \left(i(x, y) - \bar{i}\right)^2. \quad (9)$$

Autocorrelation (Vollath, 1987; 1988).

$$f_{\text{auto\_corr}} = \sum_{\text{height}} \sum_{\text{width}} i(x, y) \cdot i(x+1, y) - \sum_{\text{height}} \sum_{\text{width}} i(x, y) \cdot i(x+2, y). \quad (10)$$

Standard deviation-based correlation (Vollath, 1987, 1988).

$$f_{\text{stddev\_corr}} = \sum_{\text{height}} \sum_{\text{width}} i(x, y) \cdot i(x+1, y) - H \cdot W \cdot \bar{i}^2. \quad (11)$$

Histogram-based algorithms

Range algorithm (Firestone et al., 1991). Denote the number of pixels with intensity i by $h(i)$, the objective function is

$$f_{\text{range}} = \max\{i \mid h(i) > 0\} - \min\{i \mid h(i) > 0\} \quad (12)$$

Entropy algorithm (Firestone et al., 1991).

$$f_{\text{entropy}} = -\sum_i p_i \cdot \log_2(p_i), \quad (13)$$

where $p_i = h(i)/H \cdot W$.

Intuitive algorithms

Thresholded content (Mehdelsohn & Mayall, 1972; Groen et al., 1985). Objective function of this algorithm is the sum of intensities above a certain threshold.

$$f_{\text{thre\_cont}} = \sum_{\text{height}} \sum_{\text{width}} i(x, y), \quad (14)$$

where $i(x, y) \geq v$.

Thresholded pixel count (Groen et al., 1985).

$$f_{\text{pixel\_count}} = \sum_{\text{height}} \sum_{\text{width}} c\left(i(x, y), v\right), \quad (15)$$

where

$$c\left(i(x, y), v\right) = \begin{cases} 1, & i(x, y) \leq v \\ 0, & else \end{cases}$$

Image power (Santos et al., 1997).

$$f_{\text{power}} = \sum_{\text{height}} \sum_{\text{width}} i(x, y)^2, \quad (16)$$

where $i(x, y) \geq v$.

Dynamic search of objective function extremum

To search for the focus position of a sample, the maximum/minimum (i.e. extremum) value of the focus objective function must be precisely located. In this study, the Fibonacci search algorithm (Beveridge & Schechter, 1970) was selected for conducting the extremum search of the objective function. Under the unimodality assumption of the objective function, the Fibonacci search algorithm has been proven to be the optimal algorithm for search problems (Kiefer, 1953; Johnson, 1956) and requires the least number of computations of objective functions for autofocusing applications (Krotkov, 1987; Yeo *et al.*, 1993).

Fibonacci sequence consists of a series of Fibonacci numbers F_n, which is constructed with the recursive equation $F_n = F_{n-1} + F_{n-2}$ $(n > 1)$ and the boundary condition $F_0 = F_1 = 1$. In Fibonacci search, the length of the initial search space is taken as a Fibonacci number. The search space is subdivided according to the Fibonacci sequence. When the length of the initial search space is not a Fibonacci number, the smallest Fibonacci number greater than the length of the initial search space is used to subdivide the search space proportionally.

The algorithm flow is described in Fig. 3 where all focus objective functions are assumed to have peaks with global maxima. The objective functions with global minima will be inverted. In Fig. 3, the search space is denoted by $[a_k, b_k]$, where k is the iterative search index; N is the least index of Fibonacci sequence such that $F_N \geq b_1 - a_1$; f is the focus objective function; x_k^1 and x_k^2 are the search positions to which the z-motor should be moved and where images should be acquired to compute the objective functions. One can see from Fig. 3 that only one computation of the objective function is required for all search iterations except the first iteration. As will be discussed in the Experimental Results and Discussion section, the computation time of all the 16 focus algorithms is within 30 ms, and only 16 computations of focus objective functions were required throughout the autofocusing processes. Thus, the dynamic focusing time is mainly determined by the physical run time of the z-motor to move from its initial position to the final focus position.

Ranking methodology

A new ranking methodology is used for dynamically and statically evaluating the selected 16 focus algorithms on pap and blood smear samples. The first two criteria (i.e. dynamic accuracy and dynamic repeatability) assess the dynamic performance of a focus algorithm and the dynamic focusing system. The other five criteria previously used by Sun *et al.* (2004) and Liu *et al.* (2006) comprehensively evaluate the static performance of focus algorithms. In order to quantitatively compare the 16 focus algorithms, all focus curves were normalized, and the curves with global minimum inverted.

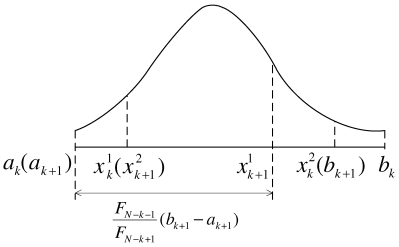

$a_1 \leftarrow$ start of search range
$b_1 \leftarrow$ end of search range
for $k = 1, \ldots, N\text{-}1$ do
  if $k = 1$ then
    $x_k^1 \leftarrow a_k + \frac{F_{N-k-1}}{F_{N-k+1}}(b_k - a_k)$
    $x_k^2 \leftarrow b_k - \frac{F_{N-k-1}}{F_{N-k+1}}(b_k - a_k)$
  endif
  if $f(x_k^1) < f(x_k^2)$ then
    $a_{k+1} \leftarrow x_k^1$
    $b_{k+1} \leftarrow b_k$
    $x_{k+1}^1 \leftarrow x_k^2$
    $x_{k+1}^2 \leftarrow b_{k+1} - \frac{F_{N-k-1}}{F_{N-k+1}}(b_{k+1} - a_{k+1})$
  else
    $a_{k+1} \leftarrow a_k$
    $b_{k+1} \leftarrow x_k^2$
    $x_{k+1}^2 \leftarrow x_k^1$
    $x_{k+1}^1 \leftarrow a_{k+1} + \frac{F_{N-k-1}}{F_{N-k+1}}(b_{k+1} - a_{k+1})$
  endif
endfor
if $f(x_k^1) > f(x_k^2)$ then
  return x_k^1
else
  return x_k^2
endif

Fig. 3. Fibonacci search algorithm.

Dynamic accuracy

Previous research (Santos *et al.*, 1997; Sun *et al.*, 2004; Liu *et al.*, 2006) studied the static accuracy of an objective function curve to describe the accuracy of the focus algorithm. However, dynamic search accuracy was not investigated; therefore, the focusing accuracy of the complete dynamic system was not represented. Considering the dynamic Fibonacci search error, the dynamic accuracy criterion proposed in this study is defined as the distance between the real focus position, which is manually determined by a proficient microscopy operator, and the maximum position dynamically located by the Fibonacci search method. To minimize the effect of random errors, 10 autofocusing trials were conducted for each pap and blood smear sample using each focus algorithm, and the averaged value represents the final dynamic accuracy.

Dynamic repeatability

This criterion assesses the repeatability of dynamic autofocusing, which is described by the standard deviation of

the located focus positions of the 10 autofocusing trials. For an ideal focus objective function, the Fibonacci search algorithm would precisely locate the same maximum position every time. In practice, the lower this measure is, the easier the same maximum position can be reached in different autofocusing trials.

Number of local maxima

Local maxima may trap the autofocusing algorithm and increase the computational complexity. This criterion represents the number of local maxima in a focus curve. The less this measure is, the easier and faster it is to reach the global maximum.

Range

This criterion measures the distance between two neighbouring local minima around the global maximum. A larger range measure permits easier searching for the maximum of the focusing curve.

Noise level

This criterion describes the speed of the direction changes (second derivative of the focusing curve) between local maxima. The sum of squared second derivatives except the value at the maximum is used to quantitatively represent this measure. A focus curve with a lower noise level prevents the Fibonacci search from being trapped into an erroneous search range and therefore, guarantees the autofocusing accuracy.

Width at 50% maximum

This criterion measures the width at 50% maximum of the focus curve (Fig. 4). The smaller it is, the sharper the focus peak is, and the easier it is to locate the focus position accurately.

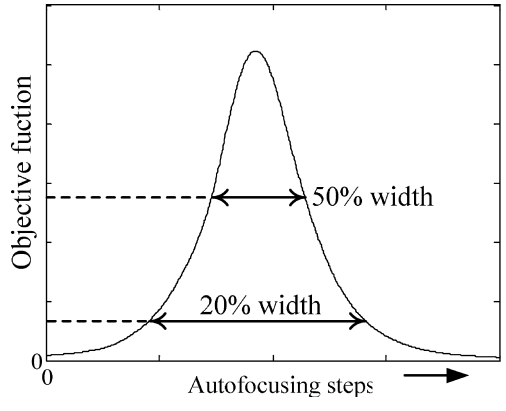

Fig. 4. Objective function curve of the focus algorithms.

Width at 20% maximum

The width at 20% maximum (Fig. 4) is employed to evaluate the performance of focus algorithms, which is of great importance for providing Fibonacci search with reliable cues of function values in a wide range to precisely locate the global maximum (Groen *et al.*, 1985).

Overall score

The ideal values for the above seven individual criteria (two dynamic criteria and five static criteria) are described in Table 1, in which the ideal values for the *range* and the *20% width criteria* are the total number of static images in each image set (800 in this study for each image set). To evaluate a focus algorithm, the difference/distance between each criterion's ideal value and the value of the focus curve is calculated. An ideal focus curve has criterion distance coordinates of [0, 0, 0, 0, 0, 0, 0]. The lower a criterion distance, the better the performance of an algorithm under this criterion. In this study, all the individual criterion distances are normalized in order to maintain equal weights for each criterion distance. The overall score is defined as the Euclidean distance of a focus curve to [0, 0, 0, 0, 0, 0, 0].

Experimental results and discussion

In both dynamic and static evaluation, the 16 focus algorithms were applied to full images (640 × 480) for computing focus objective functions. The computation time of all the 16 algorithms is within 30 ms. The selected threshold values for algorithms (14), (15) and (16) are 150, 170 and 180, respectively, which were selected because the algorithms provided their best performance with these threshold values. It has been demonstrated that algorithms (1), (2) and (3) do not require thresholding (Sun *et al.*, 2004). According to the dimension of the smallest sample feature, scale σ in algorithm (7) was set to be 1 pixel.

For dynamic evaluation, 10 experimental autofocusing trials were conducted for each sample using each focus algorithm (10 smear samples and 16 focus algorithms), amounting to 1600 dynamic autofocusing trials. The initial search space for Fibonacci search was set to be symmetrical around the real focus position, and its length (i.e. $b_1 - a_1$) was set to be 800 steps with a step size of 0.25 μm. Thus, $N = 15$ and $F_N = 987$. The speed of the z-motor was set at 70 μm/s. Figure 5 shows two representative dynamic focusing curves selected from the 1600 experimental trials. It can be seen that the search range of Fibonacci search rapidly narrowed and converged to the located focus position. The total position changes and run time of the z-motor for all searches that converged to the real focus position were fairly close. The focusing time of the 16 focus algorithms for blood and pap smears is summarized in Table 2, in which every

Table 1. Ideal values for individual ranking criteria.

Criteria	Dynamic accuracy	Dynamic repeatability	No. of local max	Range	Noise level	50% width	20% width
Ideal value	0	0	0	800	0	0	800

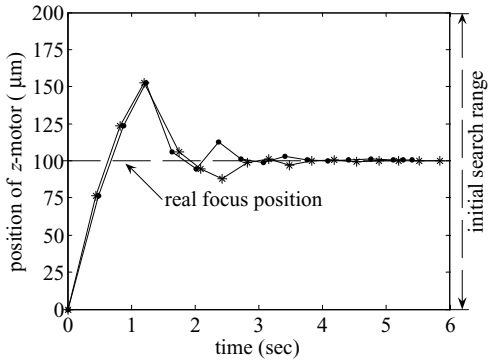

Fig. 5. Two representative dynamic focusing curves of variance algorithm (8) using Fibonacci search.

Table 2. Dynamic focusing time of blood and pap smears.

Algorithm	Focusing time of blood smears (s)	Focusing time of pap smears (s)
ThreAbsGrad (1)	5.58	5.66
SquaGrad (2)	5.62	5.71
BrennerGrad (3)	5.49	5.48
TeneGrad (4)	5.69	5.54
EnergyLapl (5)	5.53	5.41
SumModiLapl (6)	5.68	5.59
SumGausDeri (7)	5.43	5.50
Variance (8)	5.29	5.41
NormVariance (9)	5.32	5.41
AutoCorr (10)	5.54	5.50
StanDeviCorr (11)	5.38	5.40
Range (12)	5.47	5.34
EntrAlgo (13)	5.49	5.53
ThreCont (14)	5.68	5.56
ThrePixeCont (15)	5.58	5.24
ImagePower (16)	5.35	5.33

entry is the average value of 50 dynamic focusing trials. No significant differences were observed in focusing time among focus algorithms (5.24–5.71 s).

For static evaluation, a total of 8000 images collected from the 10 blood smear and pap smear samples (Fig. 1) at each step of 0.25 μm were processed using the 16 selected focusing algorithms. According to individual criteria and the overall score, the 16 algorithms were scored and ranked based on both their dynamic performance and their static focus curves of blood smear and pap smear. The evaluation results are listed in Tables 3 and 4. Every entry in column no. 2 and 3 represents the average value from 50 experimental trials for each type of samples. Every entry in column no. 4 to column no. 8 represents the average value from five focus curves. Smaller values in all columns of Tables 3 and 4 represent better performance. The numbers in parentheses show the ranking of a focus algorithm according to individual criterion distances (column no. 2–8) or the overall score (column no. 9).

From Tables 3 and 4, it can be seen that the variance algorithm (8) provides the best overall performance for both blood and pap smear samples, and that the normalized variance algorithm (9) provides almost optimal overall performance for both types of samples. This finding is in agreement with our previous study on autofocusing of blood and pap smear samples, in which only the static performance of the focus algorithms was considered (Liu *et al.*, 2006). Figure 6 shows the focus curves of the variance algorithm (8) on 10 image sets of blood and pap smear samples. One reason that explains the best overall performance of the algorithms (8) and (9) is that these statistical-based algorithms are less noise sensitive. The property of noise insensitivity enables these algorithms to produce the lowest number of local maxima, the best range and the almost lowest noise level. The contributions of these three individual criteria are clearly reflected in the best overall scores.

Together with our previously reported results (Sun *et al.*, 2004; Liu *et al.*, 2006), the variance or the normalized variance algorithm has been demonstrated to provide the best overall performance for non-fluorescence microscopy applications including pap smear and blood smear samples.

The dynamic accuracy includes the static accuracy determined by the focus algorithm and the maximum search error generated by Fibonacci search. The static accuracy was computed and ranked in Table 5 (column no. 3 and 6), which is described by the distance between the real focus position and the maximum of the static focus curve. The Fibonacci search error is listed and ranked in column no. 4 and no. 7 in Table 5, which is the absolute difference between dynamic accuracy and static accuracy. It was found that an important factor influencing the Fibonacci search accuracy is the noise level (column no. 6 in Tables 3 and 4). Of the algorithms that rank from 11th to 16th in terms of the Fibonacci search error (Table 5), four algorithms (5, 6, 10 and 12) have the highest noise level for blood smear samples and five algorithms for pap smear samples (5, 6, 10, 12 and 15). A higher noise level in

Table 3. Blood smear: ranking of 16 focus algorithms according to individual criteria and overall score.

Algorithm	Dynamic accuracy	Dynamic repeatability	No. of local max	Range	Noise level	50% width	20% width	Overall score
ThreAbsGrad (1)	2.48 (4)	0.5715 (4)	199.8 (11)	636.0 (5)	0.002530 (10)	61.0 (5)	669.6 (13)	1.5002 (8)
SquaGrad (2)	2.38 (2)	0.2518 (1)	209.4 (13)	653.6 (9)	0.010503 (12)	31.2 (1)	724.4 (15)	1.5802 (12)
BrennerGrad (3)	2.76 (5)	1.3140 (8)	200.8 (12)	636.4 (6)	0.002960 (11)	55.6 (4)	679.6 (14)	1.5108 (9)
TeneGrad (4)	2.44 (3)	0.2826 (2)	199.6 (10)	623.6 (4)	0.001540 (9)	51.4 (3)	734.2 (16)	1.5468 (10)
EnergyLapl (5)	110.96 (15)	11.4070 (12)	232.8 (16)	787.2 (13)	0.092180 (15)	201.0 (11)	439.4 (8)	1.8800 (14)
SumModiLapl (6)	110.74 (14)	13.1570 (13)	219.0 (15)	792.2 (15)	0.027650 (14)	190.4 (10)	453.2 (9)	1.7865 (13)
SumGausDeri (7)	2.26 (1)	2.2090 (9)	171.8 (8)	690.2 (12)	0.000954 (5)	212.6 (13)	396.6 (5)	1.3372 (6)
Variance (8)	4.48 (7)	0.4262 (3)	0 (1)	0 (1)	0.000058 (1)	269.2 (14)	264.8 (2)	0.6560 (1)
NormVariance (9)	4.50 (8)	0.6189 (5)	0 (1)	0 (1)	0.000117 (3)	170.2 (8)	420.8 (7)	0.6759 (2)
AutoCorr (10)	80.00 (12)	2.7616 (10)	209.8 (14)	675.0 (10)	0.017540 (13)	34.6 (2)	522.8 (11)	1.5640 (11)
StanDeviCorr (11)	43.30 (11)	38.2990 (14)	170.8 (7)	683.4 (11)	0.000957 (7)	211.4 (12)	400.2 (6)	1.4646 (7)
Range (12)	96.18 (13)	74.1220 (16)	173.6 (9)	787.4 (14)	0.175210 (16)	461.4 (15)	135.2 (1)	2.2323 (16)
EntrAlgo (13)	131.24 (16)	50.6830 (15)	26.4 (3)	792.6 (16)	0.000087 (2)	495.2 (16)	285.0 (3)	1.9066 (15)
ThreCont (14)	6.30 (9)	6.8019 (11)	161.2 (6)	647.8 (8)	0.000392 (4)	158.6 (7)	478.4 (10)	1.3023 (4)
ThrePixeCont (15)	2.76 (5)	1.2419 (7)	122.2 (4)	636.6 (7)	0.000956 (6)	95.4 (6)	646.2 (12)	1.3245 (5)
ImagePower (16)	6.58 (10)	0.7196 (6)	123.2 (5)	556.0 (3)	0.000962 (8)	190.2 (9)	393.6 (4)	1.1034 (3)

a focus curve guides Fibonacci search to a false search range and therefore, results in greater search errors. A high noise level also causes poor performance in dynamic repeatability (column no. 3 in Tables 3 and Table 4: algorithms 5, 6, 10, 12 for both blood smears and pap smears). Another factor that can prevent Fibonacci search from precisely locating the maximum is the appearance of multiple modalities. For example, despite the almost lowest noise level for both blood and pap smears in the focus curves of the Entropy Algorithm (13), the non-unimodality features [Fig. 7: curve (A)–(E) for blood smears and curve (A) and (E) for pap smears] result in poor Fibonacci search accuracy (column no. 4 and 7 in Table 5) for both blood smear samples (ranking no. 11) and pap smear samples (ranking no. 12).

Conclusion

This paper presented a comparison study with the objective of determining the optimal autofocus algorithm for bright-field imaging of blood smear and pap smear samples. The dynamic

Table 4. Pap smear: ranking of 16 focus algorithms according to individual criterion and overall score.

Algorithm	Dynamic accuracy	Dynamic repeatability	No. of local max	Range	Noise level	50% width	20% width	Overall score
ThreAbsGrad (1)	2.94 (3)	0.3597 (6)	203.4 (6)	666.6 (5)	0.002430 (8)	27.6 (5)	720.8 (14)	1.4917(8)
SquaGrad (2)	3.78 (7)	0.3226 (5)	230.6 (12)	763.4 (9)	0.029510 (13)	20.8 (1)	401.0 (10)	1.4207(5)
BrennerGrad (3)	4.24 (8)	0.3008 (3)	205.4 (7)	676.4 (6)	0.002680 (9)	26.8 (4)	720.6 (13)	1.5026(9)
TeneGrad (4)	3.64 (6)	0.2380 (2)	209.6 (9)	663.6 (4)	0.002950 (10)	25.6 (3)	751.2 (15)	1.5280(11)
EnergyLapl (5)	75.04 (14)	29.9190 (13)	263.6 (16)	788.0 (14)	0.031970 (14)	53.4 (7)	272.6 (2)	1.6223(13)
SumModiLapl (6)	131.58 (16)	61.2530 (14)	260.0 (15)	794.2 (16)	0.012100 (12)	369.4 (15)	308.4 (4)	2.1310(16)
SumGausDeri (7)	2.70 (2)	1.6977 (10)	227.2 (11)	781.0 (12)	0.000879 (5)	224.8 (12)	328.6 (6)	1.4915(7)
Variance (8)	2.42 (1)	0.1476 (1)	10.6 (1)	69.6 (1)	0.000127 (2)	201.8 (10)	314.0 (5)	0.6664(1)
NormVariance (9)	2.96 (4)	0.3159 (4)	10.8 (2)	69.6 (1)	0.000292 (4)	136.4 (9)	422.6 (11)	0.6669(2)
AutoCorr (10)	95.28 (15)	69.7470 (15)	234.0 (14)	723.0 (8)	0.035790 (15)	21.2 (2)	751.6 (16)	1.9700(15)
StanDeviCorr (11)	3.58 (5)	1.1611 (8)	226.4 (10)	780.2 (11)	0.000884 (6)	223.6 (11)	328.6 (6)	1.4880(6)
Range (12)	69.86 (13)	84.7850 (16)	167.8 (5)	774.4 (10)	0.145960 (16)	73.4 (8)	75.4 (1)	1.9189(14)
EntrAlgo (13)	18.00 (12)	1.3655 (9)	53.0 (3)	679.4 (7)	0.000076 (1)	395.8 (16)	279.6 (3)	1.3891(4)
ThreCont (14)	11.50 (11)	7.9903 (12)	208.6 (8)	787.8 (13)	0.000256 (3)	265.0 (14)	351.4 (8)	1.5145(10)
ThrePixeCont (15)	7.68 (10)	0.8725 (7)	98.6 (4)	644.8 (3)	0.003300 (11)	50.6 (6)	704.0 (12)	1.3026(3)
ImagePower (16)	5.96 (9)	1.9453 (11)	233.2 (13)	792.0 (15)	0.000888 (7)	243.2 (13)	365.0 (9)	1.5470(12)

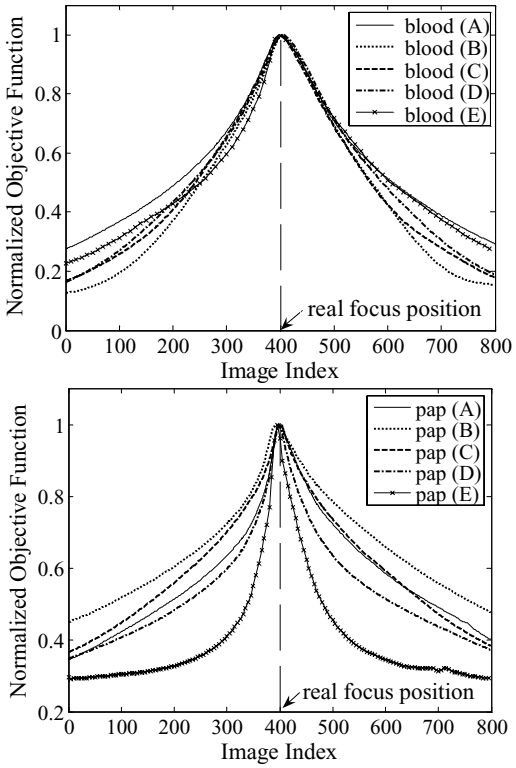

Fig. 6. Focus curves of variance algorithm (8) for 10 image sets of blood smears (top) and pap smears (bottom).

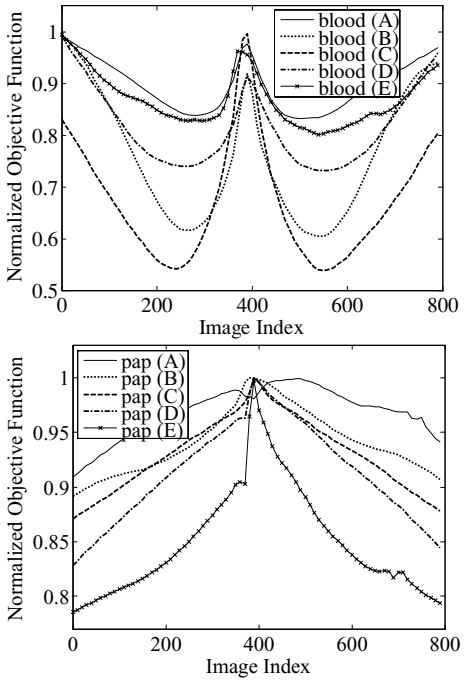

Fig. 7. Focus curves of the Entropy algorithm (13) for 10 image sets of blood smears (top) and pap smears (bottom).

autofocusing performance of 16 selected focus algorithms was, for the first time, evaluated and ranked. Fibonacci search was introduced for implementing the dynamic maximum search of the focus objective functions. A ranking methodology was employed for ranking the focusing algorithms, consisting of two newly proposed dynamic measures, five previously presented static criteria and one overall score. The variance algorithm was found to provide the best overall performance for both blood smear and pap smear samples, which is thus, appropriate to choose for automated microscopic diagnosis of blood and pap smear.

Table 5. Static accuracy and Fibonacci search error of the 16 focus algorithms for blood and pap smears.

	Blood smear			Pap smear		
Algorithm	Dynamic accuracy	Static accuracy	Fibonacci search error	Dynamic accuracy	Static accuracy	Fibonacci search error
ThreAbsGrad (1)	2.48 (4)	3.0 (1)	0.52 (3)	2.94 (3)	4.0 (7)	1.06 (7)
SquaGrad (2)	2.38 (2)	3.2 (5)	0.82 (7)	3.78 (7)	6.4 (12)	2.62 (9)
BrennerGrad (3)	2.76 (5)	3.0 (1)	0.24 (1)	4.24 (8)	4.0 (7)	0.24 (2)
TeneGrad (4)	2.44 (3)	3.0 (1)	0.56 (4)	3.64 (6)	4.2 (10)	0.56 (5)
EnergyLapl (5)	110.96 (15)	15.6 (15)	95.36 (15)	75.04 (14)	8.6 (14)	66.44 (14)
SumModiLapl (6)	110.74 (14)	10.8 (13)	99.94 (16)	131.58 (16)	7.0 (13)	124.58 (16)
SumGausDeri (7)	2.26 (1)	6.2 (11)	3.94 (10)	2.70 (2)	2.2 (1)	0.5 (4)
Variance (8)	4.48 (7)	3.8 (8)	0.68 (5)	2.42 (1)	2.6 (4)	0.18 (1)
NormVariance (9)	4.50 (8)	3.4 (6)	1.10 (8)	2.96 (4)	2.6 (4)	0.36 (3)
AutoCorr (10)	80.00 (12)	3.4 (6)	76.6 (13)	95.28 (15)	4.0 (7)	91.28 (15)
StanDeviCorr (11)	43.30 (11)	6.2 (11)	37.10 (12)	3.58 (5)	2.2 (1)	1.38 (8)
Range (12)	96.18 (13)	12.2 (14)	83.98 (14)	69.86 (13)	5.6 (11)	64.26 (13)
EntrAlgo (13)	131.24 (16)	145.0 (16)	13.76 (11)	18 (12)	22.8 (16)	4.8 (12)
ThreCont (14)	6.30 (9)	5.0 (9)	1.30 (9)	11.50 (11)	10.6 (15)	0.9 (6)
ThrePixeCont (15)	2.76 (5)	3.0 (1)	0.24 (1)	7.68 (10)	3.2 (6)	4.48 (11)
ImagePower (16)	6.58 (10)	5.8 (10)	0.78 (6)	5.96 (9)	2.2 (1)	3.76 (10)

References

Angulo, J. & Flandrin, G. (2003) Automated detection of working area of peripheral blood smears using mathematical morphology. *Anal. Cell. Pathol.* **25**, 37–49.

Beveridge, G.S. & Schechter, R.S. (1970) *Optimization: Theory and Practice*, McGraw-Hill, New York.

Brenner, J., Dew, B., Horton, J., King, J., Neirath, P. & Sellers, W. (1971) An automated microscope for cytologic research. *J. Histochem. Cytochem.* **24**, 100–111.

Firestone, L., Gook, K., Gulp, K., Talsania, N. & Preston, K. (1991) Comparison of autofocus methods for use in automated algorithms. *Cytometry* **12**, 195–206.

Geusebroek, J.M., Cornelissen, F., Smeulders, A. & Geerts, H. (2000) Robust autofocusing in microscopy. *Cytometry* **39**, 1–9.

Groen, F., Young, I.T. & Ligntart, G. (1985) A comparison of different focus functions for use in autofocus algorithms. *Cytometry* **6**, 81–91.

Johnson, S.M. (1956) *Best Exploration for Maximum is Fibonaccian. RAND Corporation Report P-856*. Santa Monica, CA.

Kiefer, J. (1953) Sequential minimax search for a maximum. *Proc. Am. Math. Soc.* **4**, 502–506.

Krotkov, E. (1987) Focusing. *Int. J. Comput. Vis.* **1**, 223–237.

Liu, X.Y., Wang, W.H. & Sun, Y. (2006) Autofocusing for automated microscopic evaluation of blood smear and pap smear. *IEEE International Conference of the Engineering in Medicine and Biology Society*, Aug. 30–Sept. 3 2006, New York, USA.

Mehdelsohn, M.L. & Mayall, B.H. (1972) Computer-oriented analysis of human chromosomes – III focus. *Comput. Biol. Med.* **2**, 137–150.

Nayar, S. & Nakagawa, Y. (1994) Shape from focus. *IEEE Trans. Pattern Anal. Machine Intell.* **16**, 824–831.

Santos, A., Solórzano, C.O., Vaquero, J.J., Peña, J.M., Malpica, N. & Pozo, F. (1997) Evaluation of autofocus functions in molecular cytogenetic analysis. *J. Microsc.* **188**, 264–272.

Simon, H., Voss, K., Wenzelides, K., Hufnagl, P. & Roth, K. (1986) Automated microscopic image evaluation for histological diagnosis of tumours. *Exp. Pathol.* **30**, 51–58.

Subbarao, M., Choi, T. & Nikzad, A. (1993) Focusing techniques. *Opt. Eng.* **32**, 2824–2836.

Sun, Y., Duthaler, S. & Nelson, B.J. (2004) Autofocusing in computer microscopy: selecting the optimal focus algorithm. *Microsc. Res. Tech.* **65**, 139–149.

Vollath, D. (1987) Automatic focusing by correlative methods. *J. Microsc.* **147**, 279–288.

Vollath, D. (1988) The influence of the scene parameters and of noise on the behavior of automatic focusing algorithms. *J. Microsc.* **151**, 133–146.

Yeo, T., Jayasooriah, S.O. & Sinniah, R. (1993) Autofocusing for tissue microscopy. *Image Vis. Comput.* **11**, 629–639.

